

Yuxuan Yang, Joe J. Mohr & Tim O'Hara  
*Univ. of Illinois*

# **DENSITY PROFILE AND X-RAY LUMINOSITY FUNCTION OF AGNs IN GALAXY CLUSTERS**

# AGN feed back in clusters: radio and X-ray selected AGNs

Radio loud AGNs are found to prefer clusters environment. They are capable of converting kinetic energy in the radio jets to heat the ICM. What makes radio loud AGNs so special in clusters? Can radio quiet AGNs also contribute to heating the IGM?

How does cluster environment affect the evolution of supermassive blackholes?

Studying both radio and X-ray selected AGNs in and near galaxy clusters may provide useful clues to both questions

# Previous studies

Optically selected emission line AGNs: Rarer in clusters than in lower density fields (Dressler et al. 1985 and reference therein).

Radio galaxies: The spatial density of radio galaxy is  $\sim 6000$  times higher than that in non-cluster fields (Lin & Mohr 2007).

X-ray selected AGNs: Excess of point sources has been seen in several individual clusters (e.g. Sun & Murray, 2002, Henry & Briel 1991, Molnar et al. 2002). Statistical studies found significant point source excess in clusters (Ruderman & Ebeling 2005, Gilmour et al. 2009, Galametz et al. 2009). A study of 35 spectroscopic complete AGNs in 8 clusters show AGN content in clusters are no lower than in the non-cluster field (Martini et al. 2007), but recently found the AGN fraction in clusters can be 10 times lower in clusters than in fields (Martini et al. 2009. Also see Hart et al. 2009).

# Cluster Sample and Control fields

The cluster sample were drawn from the Chandra archive with redshifts ranging from 0.2 – 1.3. The lower limit of redshift allows study of cluster temperatures to  $> r2500$ . The name, Obs ID and X-ray properties of the clusters can be found in O'Hara, Mohr & Sanderson (2007). We use 68 clusters from the O'Hara sample that have no neighbors in the same Chandra fields. The redshift and temperature distributions are shown in Fig. 1. The exposure time of the Chandra observations range from 5 to 170 ks, with median exposure of 25.6 ks.

To estimate completeness of source detection at large cluster-centric distances (and large off-axis angles), we also analyzed a sample of Chandra blank field observations. These include the Extended Chandra deep field south (4 ACIS-I fields, 200ks), the SWIRE Lockman Hole field (9 ACIS-I fields, 70 ks), and one observation in Groth-Westphal field (1 ACIS-I field, 90 ks).

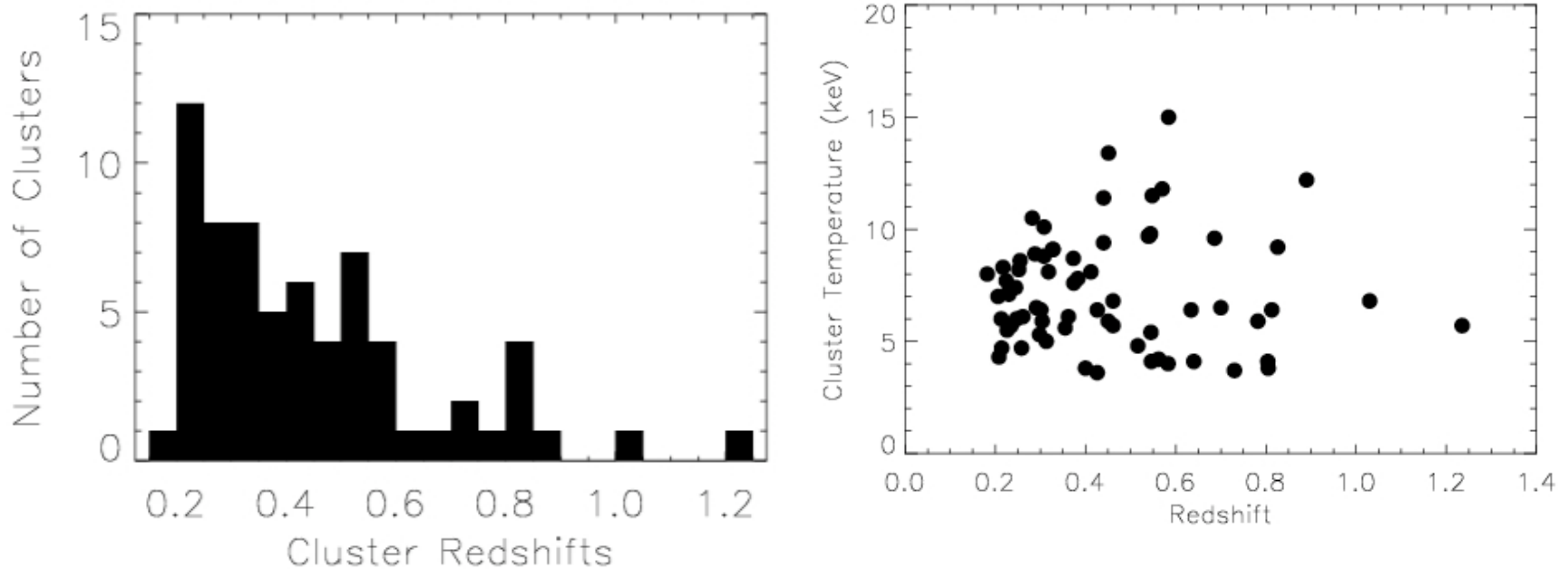


Fig. 1 Redshift (left) and X-ray temperature distribution of the sample Clusters. The median redshift of the sample is 0.38. The temperature of the clusters are higher than 3 keV . There is no bias on sample cluster temperature/mass as a function of redshift.

# Sensitivity in cluster-centric regions

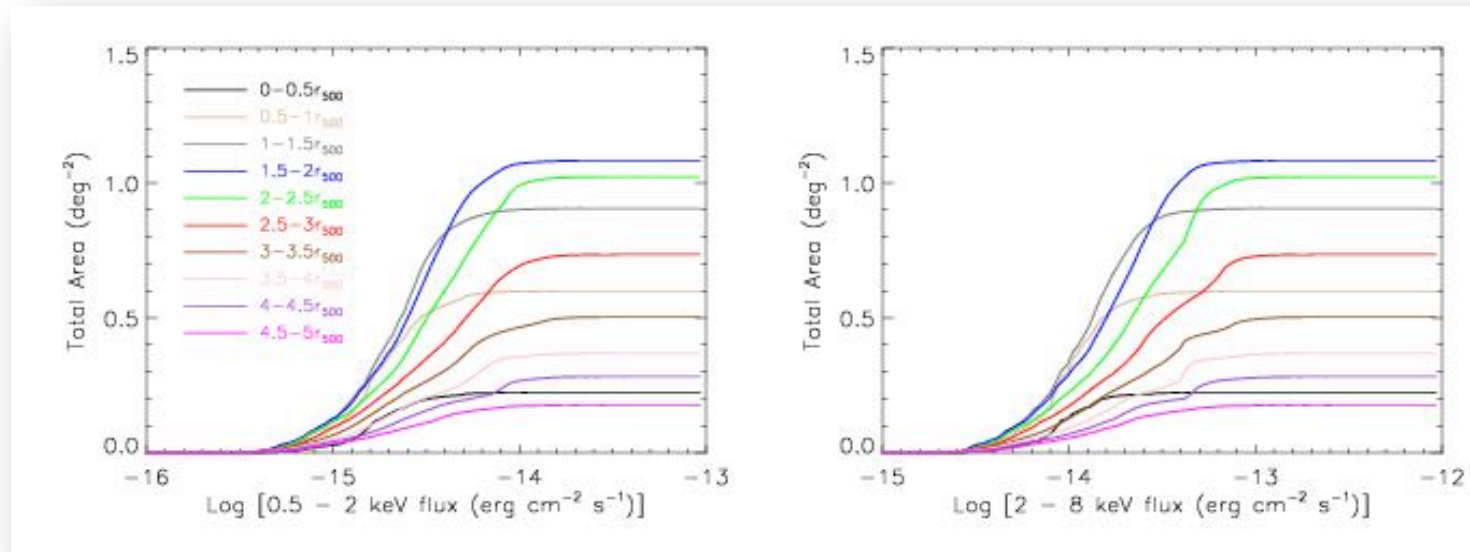


Fig 2. The effective area of the survey as a function of X-ray fluxes in 10 cluster-centric regions from 0 To  $5r_{500}$ . Left panel: 0.5-2 keV ; Right panel: 2-8 keV band. The survey is complete in all regions at flux Levels  $> 2 \times 10^{-14}$  cgs in the soft band, and  $> 6 \times 10^{-14}$  cgs in the hard band.

# Surface density distribution

● The cluster-centric distribution of AGNs in clusters are calculated in annulus regions centered on the X-ray peaks. The distances from the clusters are normalized to  $r_{200}$ . Above flux levels indicated in Fig. 3, the detection sensitivity is uniform for all regions.

● Significant excess of sources is seen at  $r < r_{200}$  compared to  $r > r_{200}$ .

● At  $r \gg r_{200}$  the surface density agrees with blank field value (Dotted lines)

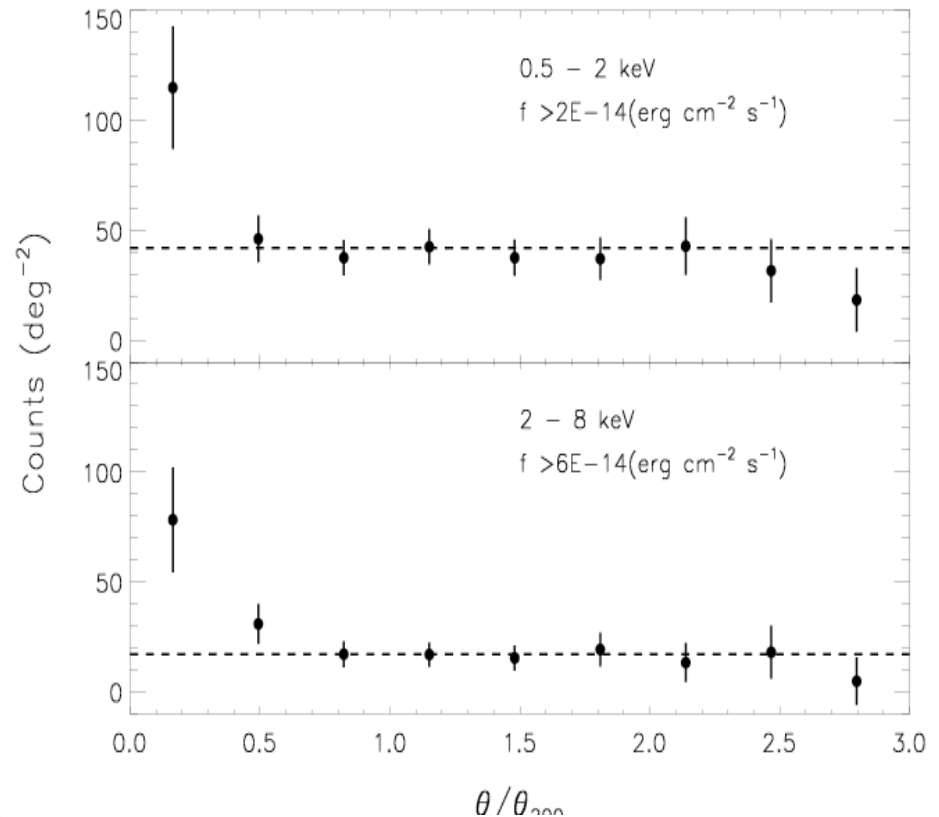


Fig. 3 Cluster-centric distribution of AGNs.

# Field LogN-LogS

We calculate differential LogN-LogS in control fields and cluster fields with  $r > r_{200}$ . Because there is no significant variation in source counts in different cluster-centric regions, we adopt the following formula to calculate the differential number counts.

$$\frac{dN}{d\text{Log}S} = \sum_{f_{\min} < f < f_{\max}} \frac{1}{\Omega(f)}$$

We found very good agreement of the LogN-LogS between control and Cluster fields (Fig. 4), which suggests

1. Our point source catalogs are complete to large off-axis angles;
2. AGN counts beyond  $r_{200}$  are consistent with those in blank fields.

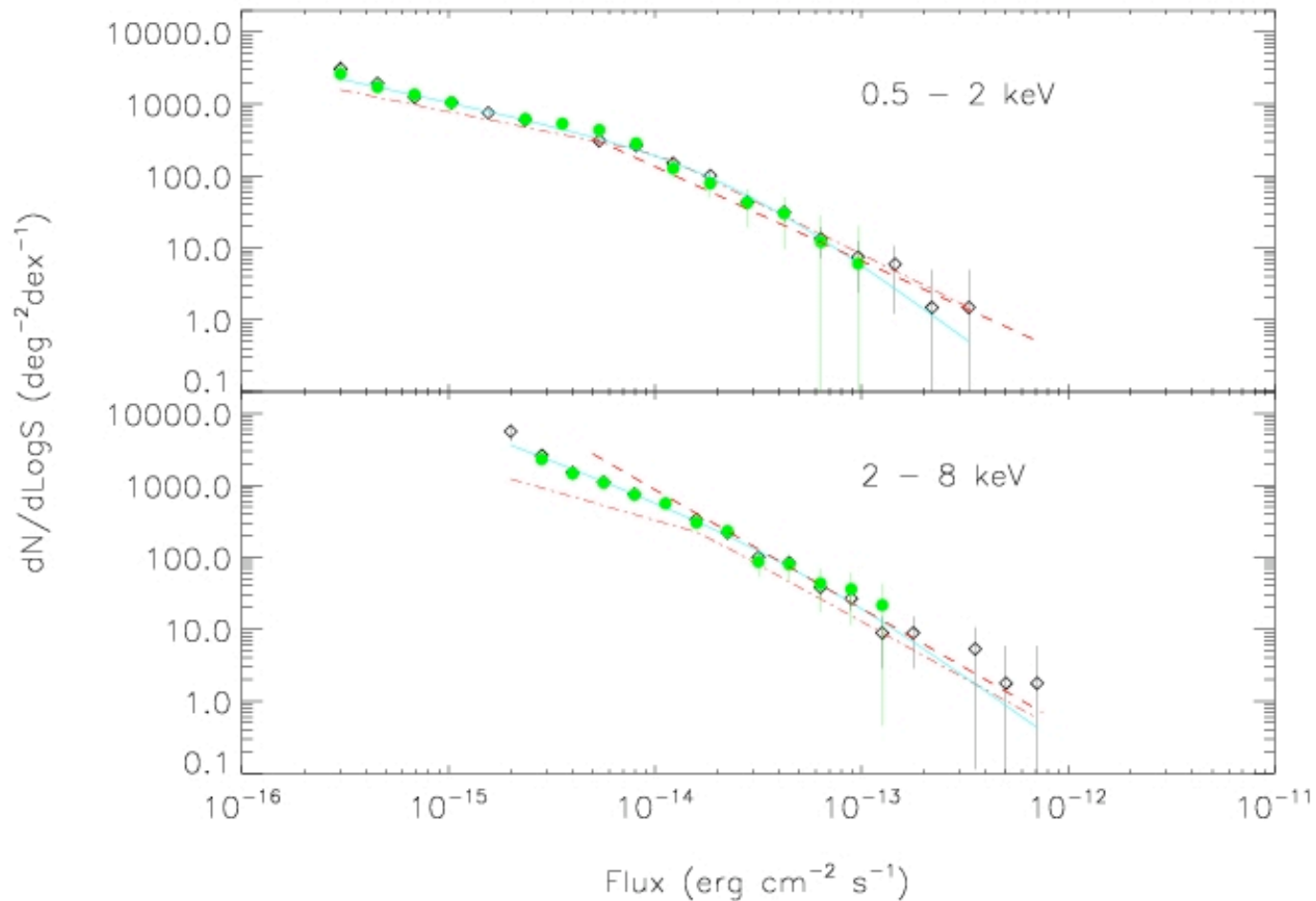


Fig. 4 Differential number counts of AGNs in control field (filled dots) and those in cluster fields with  $r > r_{200}$  (diamonds). Also plotted are the logN-logS of field AGNs. Dash-dotted: ChAMP (Kim et al. 2007). Dashed: XMM-Newton (Mateos et al. 2008).

# Deprojected radial profile

We model the radial profile of AGNs above given luminosity limits (Fig.6 ) with the NFW profile  $n(x) = n_0 x^{-1} (1+x)^{-2}$ ; where  $x = c_g r/r_{200}$ . This allow us to fit the surface density profiles with the projected NFW model. The resulting model parameters are shown below.

Result: the concentration parameter of X-ray selected AGNs agree with those of normal galaxies and are much smaller than those for radio loud AGNs (Lin et al 2007);

TABLE 1  
BEST-FIT PARAMETERS OF THE DENSITY PROFILE

| Band (keV) | $\log L_{\min} (\text{erg s}^{-1})$ | $n_0$                  | $c_g$               | $\chi^2/dof$ |
|------------|-------------------------------------|------------------------|---------------------|--------------|
| 0.5 – 2    | 42                                  | $1.50 \pm 0.40$        | $3.6^{+0.6}_{-0.3}$ | 14.0/8       |
| 0.5 – 2    | 42.5                                | $0.50^{+0.15}_{-0.35}$ | $2.7^{+0.6}_{-0.3}$ | 11.3/8       |
| 2 – 8      | 42.5                                | $0.95 \pm 0.60$        | $4.4^{+2.4}_{-0.8}$ | 14.0/8       |
| 2 – 8      | 43.0                                | $.050 \pm .03$         | $1.5^{+1.0}_{-0.3}$ | 7.0/8        |

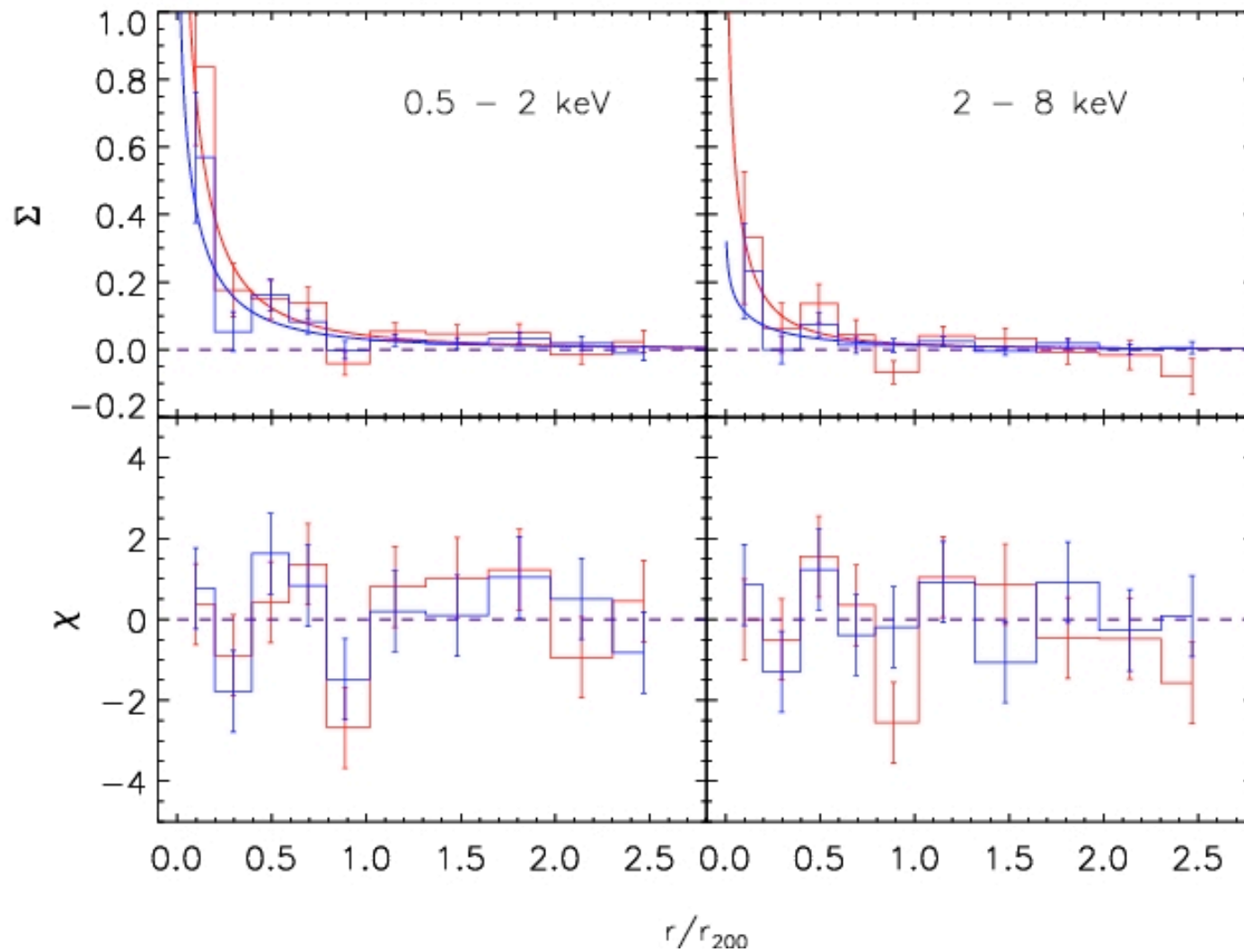


Fig.5 Radio profiles and the best-fit using projected NFW profile. Luminosity Limits:  $\text{Log } L \text{ (erg/s)} > 42.5$  for the 0.5 – 2 keV and 43 for 2-8 keV (red);  $\text{Log } L \text{ (erg/s)} > 43$  for 0.5 – 2 keV band and 43.5 for 2 – 8 keV (blue)

# Averaged Luminosity function

1. We calculate the AGN excess in each cluster within  $\theta_{200}$  as a function of luminosity using the best-fit LogN-LogS. The excess within  $r_{200}$  is calculated assuming  $c_g=3$ . Effective area as a function of flux is estimated using the sensitivity maps for that cluster. Similarly the effective volume is the effective area map integrated along the LOS that intersects the sphere with  $R = r_{200}$ . The AGN excess, and effective volume are then stacked to estimate the XLF (Fig. 6).
2. Also shown in Fig. 6 are field AGN luminosity functions scaled by  $200/\Omega_M$ , where we adopted  $\Omega_M(z=0)=0.24$ . Lin, Mohr & Stanford (2004) showed that the K-band luminosity function of cluster member galaxies within virial radii of clusters roughly scales as the over density of dark matter.
3. We found that the normalizations of the observed XLF in clusters are lower by 1.2 and 2.5  $\sigma$  in the soft and hard band than expected if the AGN fraction is the same in cluster members and field galaxies. The inferred AGN fractions are 73% and 52% of the field AGN fractions in the soft and hard bands. The difference between soft and hard band AGN fraction is only significant at  $1\sigma$  level.

## Averaged Luminosity Functions within $r_{200}$

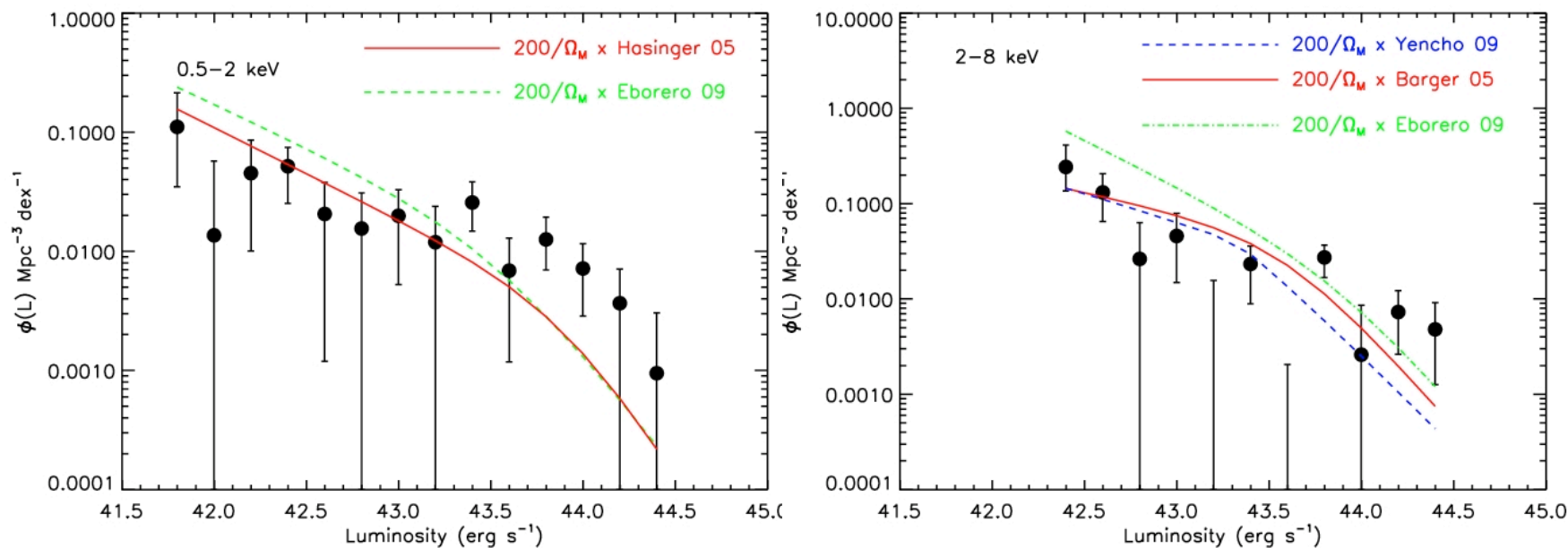
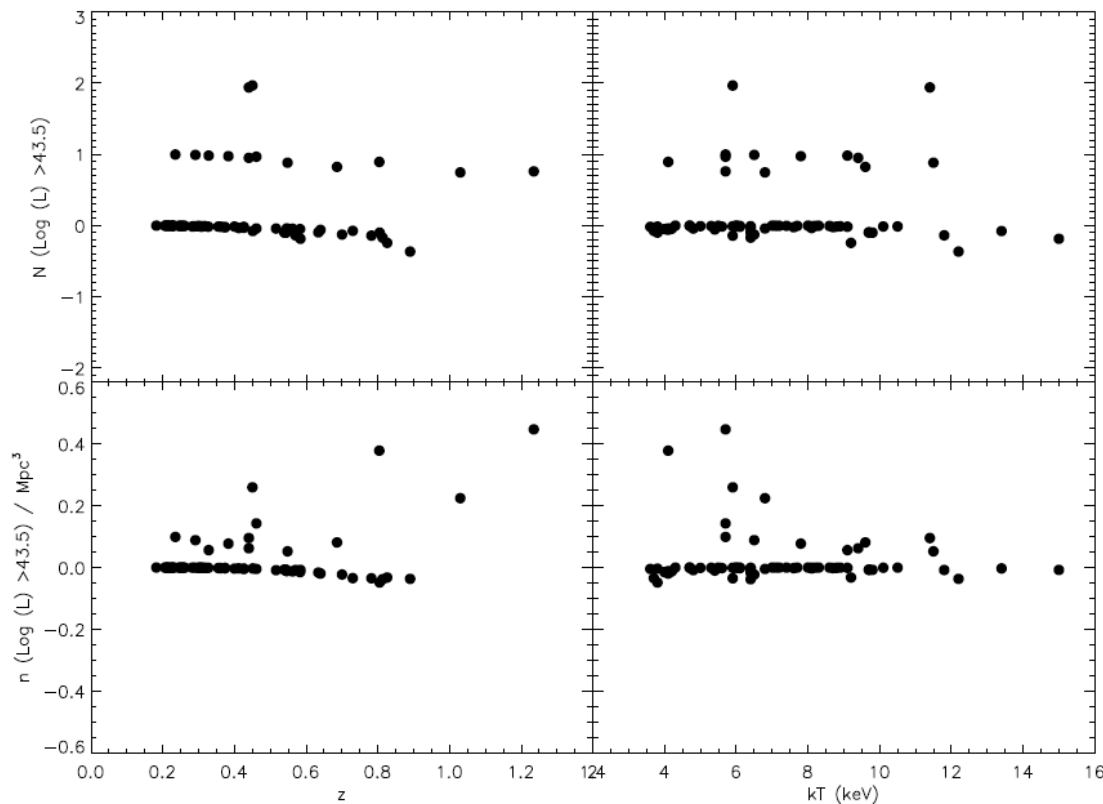


Fig. 6 Luminosity function of AGNs in clusters in soft and hard bands. If the AGN fraction in cluster members is the same as in the field galaxies, the XLF within  $r_{200}$  should match the field XLF scaled by  $200/\Omega_M(z)$ . We fit the observed XLF with  $A/\Omega_M(z) \phi_{\text{field}}$  (we chose the LF from Hasinger and Eborero to represent soft and hard field XLF) and we found  $A=147 \pm 43$  and  $105 \pm 37$  for soft and hard bands, respectively.

# Redshift and temperature dependence



To avoid selection effect we only look at point source excess in 0.5-2 keV band within  $r_{500}$  and  $\text{Log } L > 43.5$  where the survey is complete. With these constraints the number of clusters with source excess is small. No definitive conclusion can be made.

Fig. 7 The source excess and number densities above complete threshold in each cluster within  $r_{500}$ .

# Conclusions

- The surface density distribution of point sources show clear excess which is centrally peaked within  $r_{200}$  above the survey completeness. Outside  $r_{200}$ , the surface density profile is flat and agrees with the surface density in non-cluster fields.
- The deprojected radial density profile of X-ray selected AGNs shows a concentration of  $c_g = 2-4$  which agrees with that of normal galaxies rather than radio loud AGNs.
- We study of stacked XLF of AGNs within  $r_{200}$ . On average the cluster AGN XLFs are lower than that of field AGN XLFs scaled by  $200/\Omega_M(z)$ , at  $1.2$  and  $2.5\sigma$  levels for soft and hard bands respectively. This suggest the AGN fraction in clusters is  $(73 \pm 21)\%$  of the field AGN fraction in the soft band, and  $(52 \pm 18)\%$  in the hard band.

# References

1. O'Hara, T. B., Mohr, J.J., Sanderson, A. J. R., 2007, arXiv0710.5782;
2. Lin, Y-T & Mohr, J.J. 2007, ApJS, 170, 71;
3. Lin, Y-T., Mohr, J. J. & Stanford, S. A. 2007 ApJ. 610, 745;
4. Barger A. J. et al. 2005, ApJ, 129, 578;
5. Yencho B. et al. 2009, ApJ, 698, 380;
6. Hasinger G., et al. 2005, A&A, 441, 417;
7. Eborero J. et al. 2009, 493, 55;
8. Mateos, S. et al. 2008, A&A, 492, 51;
9. Gilmour R., et al. 2009, MNRAS, 392, 1509;
10. Galametz, A. et al. 2009, ArXiv eprints;
11. Ruderman & Ebling 2005, ApJL, 623, L81;
12. Martini, P., Mulchaey, J.S. & Kelson, D. D. 2007, ApJ, 664, 761;
13. Martini.P. et al. 2009 ArXiv eprints;
14. Sun, M. & Murray, S.S., 2002, ApJ. 577, 139;
15. Dressler, A., Thompson, I. B. & Sackett, S. A. 1985 ApJ. 288, 481;
16. Henry J. P. & Briel, U. G., 1991 A&A, 246, L14;
17. Molnar M.S., et al. 2002, ApJ. 573, L91;
18. Branchesi, M. et al. 2007, A&A, 462, 449;
19. Elvis et al. 1994, ApJS, 95, 1;